Materials Research Express

PAPER • **OPEN ACCESS**

Structural evolution across the metal-insulator transition of strongly distorted $Lu_{1-x}Sc_xNiO_3$ perovskites (x = 0, 0.1, 0.2)

To cite this article: Qi Cui *et al* 2020 *Mater. Res. Express* **7** 126301

Materials Research Express

OPEN ACCESS

RECEIVED
2 November 2020

REVISED
16 November 2020

ACCEPTED FOR PUBLICATION
20 November 2020

PUBLISHED
2 December 2020

PAPER

Structural evolution across the metal-insulator transition of strongly distorted $Lu_{1-x}Sc_xNiO_3$ perovskites (x = 0, 0.1, 0.2)

Qi Cui[1,2], **Ningning Wang**[1,2], **Jose A Alonso**[3,*], **François Fauth**[4] and **Jinguang Cheng**[1,2,5,*]

[1] Beijing National Laboratory for Condensed Matter Physics and Institute of Physics, Chinese Academy of Sciences, Beijing 100190, People's Republic of China
[2] School of Physical Sciences, University of Chinese Academy of Sciences, Beijing 100190, People's Republic of China
[3] Instituto de Ciencia de Materiales de Madrid, CSIC, Cantoblanco, E-28049 Madrid, Spain
[4] CELLS–ALBA Synchrotron, Cerdanyola del Valles, Barcelona, E-08290, Spain
[5] Songshan Lake Materials Laboratory, Dongguan, Guangdong 523808, People's Republic of China
[*] Authors to whom any correspondence should be addressed.

E-mail: ja.alonso@icmm.csic.es and jgcheng@iphy.ac.cn

Keywords: rare-earth nickelates, charge disproportionation, metal-insulator transition, $LuNiO_3$

Supplementary material for this article is available online

Abstract

$RNiO_3$ perovskites have been described to present thermally driven metal-insulator transitions (at T_{MI}) as a function of the rare-earth ion size (R = Pr to Lu). Aiming to extend the stability range of $RNiO_3$ for smaller R^{3+} ions, we prepared $Lu_{1-x}Sc_xNiO_3$ (x = 0, 0.1, 0.2) perovskites, being Sc^{3+} ions substantially smaller than Lu^{3+}, by using a multi-anvil high-pressure synthesis device at 10 GPa. We have studied the structural evolution of $Lu_{0.9}Sc_{0.1}NiO_3$ by synchrotron x-ray diffraction (SXRD) from room temperature to 350 °C. The symmetry of the lattice evolves from monoclinic ($P2_1/n$) to orthorhombic (*Pbnm*) upon heating across T_{MI} (≈320 °C), with the existence of two chemically and crystallographically distinct nickel sites in the insulating, monoclinic regime, whereas the metallic phase has a single NiO_6 environment. A simultaneous structural and electronic transition implies an abrupt evolution of the lattice parameters and size of the NiO_6 octahedra upon entering the metallic regime, leading to the merging of the disproportionated Ni-O bond lengths. The magnetic properties correspond to the establishment of antiferromagnetic correlations at the Ni sublattice; a decrease of the T_N ordering temperature from 122 K (x = 0) to 113 K (x = 0.2) is observed as the Sc content increases, which is concomitant with a more distorted perovskite structure.

Introduction

Rare-earth nickelates $RNiO_3$ have attracted the interest of researchers over the last three decades aiming to establish the relationships between structure and observed physical properties. While initially described in 1971 by Demazeau *et al* [1] the materials underwent a resurgence of interest after the discovery of a thermally driven metal-insulator (MI) transition depending on the rare-earth ion size [2–6]. In the case of small rare-earths (R = Ho-Lu, Y) it was subsequently shown that the symmetry of the lattice evolves from monoclinic ($P2_1/n$) to orthorhombic (*Pbnm*) upon heating across T_{MI} [7–11], with the presence of two nickel sites from the chemical and crystallographical point of view in the insulating, monoclinic regime, whereas the metallic phase has a single NiO_6 environment. The phenomenology involving MI transitions is peculiar of electron-correlated systems, and therefore $RNiO_3$ oxides have always been taken as paradigmatic examples where to investigate fundamental problems of condensed matter [12]. Moreover, their properties find applications as multiferroic oxides [13] superlattices [14–16], fuel cells [17] memory devices [18] or bio-electronic interfaces [19]. Negative magnetorresistance has been described in thin films of $NdNiO_3$ [20, 21], and superconductivity below T_C = 9–15 K for infinite-layer derivatives of composition $Nd_{0.8}Sr_{0.2}NiO_2$ [22]. First-principles electronic structure calculations show that charge ordered rare-earth nickelates of the type $RNiO_3$ (R = Ho, Lu, Pr and

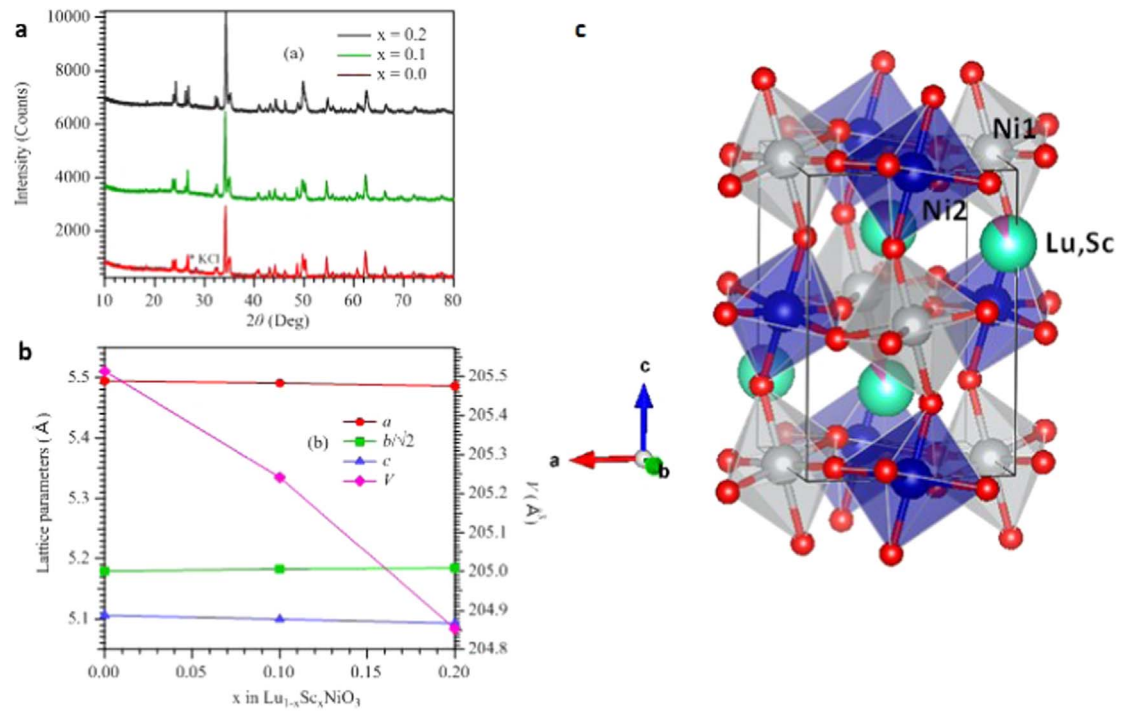

Figure 1. (a) Powder XRD patterns at 25 °C (CuKα), (b) lattice parameters after Rietveld refinement from laboratory XRD for the series of $Lu_{1-x}Sc_xNiO_3$ samples and (c) view of the crystal structure of the monoclinic $P2_1/n$ phase, with two distinct $Ni1O_6$ and $Ni2O_6$ octahedra alternating in the crystal.

Nd) are multiferroic with very large magnetically-induced ferroelectric (FE) polarizations [13]; multiferroicity has also been described in transition-metal perovskites derived from $RNiO_3$, like R_2NiMnO_6 [23, 24].

Since the first diffraction studies across the metallic-insulator transition [3–5], the observed symmetry reduction in the insulating regime [7–9] was ascribed to a charge disproportionation effect, or uncomplete charge-ordering phenomenon, where Ni^{3+} (metallic regime) evolves into $Ni^{3+\delta}$ and $Ni^{3-\delta}$ (insulating regime) located in two differently-sized NiO_6 octahedra. It is owing to the asymmetric distribution of two distinct Ni1 and Ni2 atoms coordinated in octahedra with distinct Ni–O distances [25–27]. Alternatively, the structural distortion has been interpreted as the result of a bond disproportionation: the d^8 electronic configuration is preserved in Ni atoms, whereas a positive charge is segregated at the oxygen positions, according to Ni-3*d* and O-2*p* hybridization. A configuration $3d^8L^1 \rightarrow 3d^8 + 3d^8L^2$ is ascribed to the disproportionated state, according to spectroscopic studies [26, 28, 29].

The stabilization of these materials containing Ni^{3+} becomes more difficult with the reduction in size of the rare-earth cation along the lanthanide series. After the successful preparation of $RNiO_3$ for the smallest rare-earths R = Er, Tm, Yb, Lu, at moderate pressures (2 GPa), we were able to study by neutron powder diffraction (NPD) the crystal evolution across T_{MI} (for instance, [25] for Yb and Tm, or [10] for $LuNiO_3$). Aiming to extend the stability range of $RNiO_3$ for even smaller R^{3+} ions, we proposed the preparation of $Lu_{1-x}Sc_xNiO_3$ perovskites, being Sc^{3+} ion (VIII: 0.870 Å) substantially smaller than Lu^{3+} (VIII: 0.977 Å). This involves a decrease of the tolerance factor, with an additional tilting effect of the octahedra and implying even more severe preparation conditions. This was achieved in a multianvil high-pressure synthesis device, able to reach over 10 GPa.

Moreover, these compounds exhibit antiferromagnetic magnetic structures at low temperature, arising from competing interactions at the Ni sublattice, with Néel temperatures identical to T_{MI} for larger R cations (R = Pr, Nd) whereas a lower T_N is described for R = Sm → Lu [30–33]. Additionally, some magnetic rare-earths become long-range ordered, sometimes with different periodicity, as observed for $HoNiO_3$ [32].

This work describes the preparation of these novel, extremely distorted, nickel perovskites, and the structural investigation across the MI transition of the x = 0.1 specimen, showing the evolution from the room-temperature (RT) monoclinic and insulating phase to the high-temperature orthorhombic, metallic phase. High angular resolution SXRD is required since the metric of the monoclinic unit-cell at RT involves monoclinic β angles below 90.15°, implying a strong pseudo-orthorhombic character. The magnetic properties display a reduction of the Néel temperature, which is also consistent with the increment of the structural distortion observed by diffraction methods.

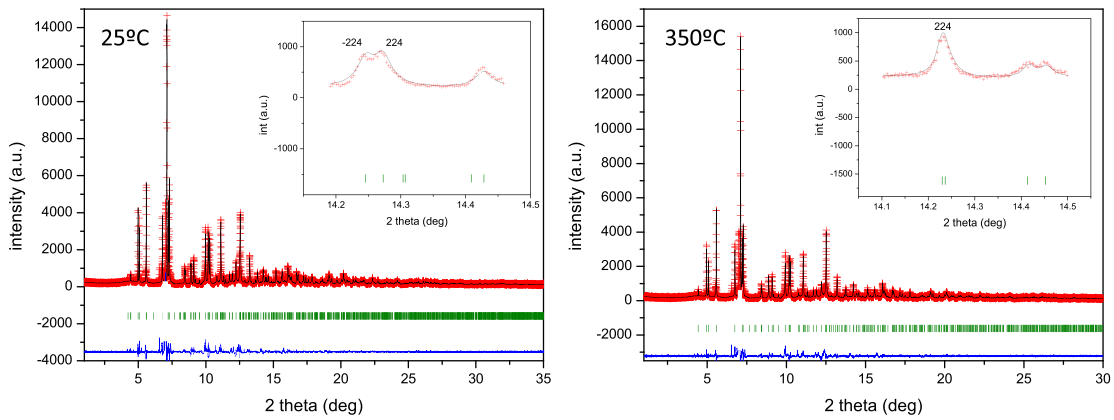

Figure 2. Rietveld plots from SXRD data of $Lu_{0.9}Sc_{0.1}NiO_3$ at (a) 25 °C and (b) 350 °C, after refinement in $P2_1/n$ and Pbnm space groups, respectively. The insets show the characteristic monoclinic splitting between (−224) and (224) reflections, which vanishes above T_{MI}. Discrepancy factors (a) at 25 °C: $R_p = 10.5\%$, $\chi^2 = 4.84$, $R_{Bragg} = 9.73\%$ (b) at 350 °C: $R_p = 10.7\%$, $\chi^2 = 2.75$, $R_{Bragg} = 10.60\%$.

Experimental

Polycrystalline samples of $Lu_{1-x}Sc_xNiO_3$ (x = 0, 0.1, 0.2) were prepared under high-pressure conditions in a Kawai-type multianvil module (Max Voggenreiter GmbH). The x = 0 perovskite, $LuNiO_3$, was prepared for comparative purposes. The starting materials (0.5-x/2)Lu_2O_3, (x/2)Sc_2O_3, and $Ni(OH)_2$ in the stoichiometry ratio are thoroughly mixed with ~30 wt.% $KClO_4$, which serves as the oxidizing agent. The precursor powders were placed in a gold capsule, sealed and set in a cylindrical graphite heater. All these sample assembly was contained in a semi-sintered octahedron made of Ceramacast 584-OF. The pressure was generated by compressing the octahedron (edge length 14mm) with eight pieces of WC anvils with a truncated edge length of 8 mm. For each synthesis, the sample was subjected to heat treatment at 900 °C for 20 min under 10 GPa. The temperature was quenched to room temperature before releasing pressure slowly. The resultant products were washed with water to dissolve KCl and then dried in air at 100 °C for 2 h. Phase purity of the obtained $Lu_{1-x}Sc_xNiO_3$ (x = 0, 0.1, 0.2) polycrystalline samples was assessed by x-ray powder diffraction (XRD) at room temperature with CuKα radiation.

SXRD patterns were collected in the powder diffraction station of the MSPD beamline at the ALBA synchrotron, Barcelona (Spain), with 38 keV energy, $\lambda = 0.3252$ Å, and with the high angular resolution MAD set-up [34]. A selected sample $Lu_{0.9}Sc_{0.1}NiO_3$ was contained in a quartz capillary of 0.5 mm diameter. The acquisition temperatures were 25 °C (RT) and 100, 150, 200, 250, 280, 300, 320 and 350 °C. The refinement of the structures was performed by the Rietveld method. DC magnetic susceptibility was measured with a commercial Magnetic Property Measurements System (MPMS-III, Quantum Design) in the temperature range 2 K ~ 300 K under an external magnetic field of 0.5 T after field-cooled from RT.

Results and discussion

Figure 1(a) shows the laboratory XRD patterns of $Lu_{1-x}Sc_xNiO_3$ (x = 0.0, 0.1, 0.2) polycrystalline raw samples. The peak marked by an asterisk is the main peak of KCl coming from $KClO_4$, which would be washed away before characterization. Lattice parameters obtained from the Rietveld refinements from laboratory XRD patterns are illustrated in figure 1(b). With increasing x in the $Lu_{1-x}Sc_xNiO_3$ series, *a* and *c* decrease, but *b* increases with a net decrease of unit-cell volume V, in line with the fact that Sc^{3+} has a smaller ionic radius than Lu^{3+}.

The crystal structure of $Lu_{0.9}Sc_{0.1}NiO_3$ at RT, in the insulating region, was refined in the monoclinic $P2_1/n$ space group. Above T_{MI}, the structure was defined in the orthorhombic *Pbnm* space group; the abrupt variation of the unit-cell parameters, particularly the monoclinic beta angle, described below, indicated $T_{MI} = 320$ °C, slightly lower than that of $LuNiO_3$, of 326 °C [10]. The SXRD patterns after the Rietveld refinement at RT and 350 °C are displayed in figure 2. The plots at the remaining temperatures are gathered in figure S1 is available online at stacks.iop.org/MRX/7/126301/mmedia of the Supplementary Information. Thanks to the excellent crystallinity and the high angular resolution of the MSPD diffractometer, it was possible to resolve certain characteristic peak splittings in the monoclinic phase, as illustrated in the insets of figure 2, for the (−2 2 4) and (2 2 4) reflections, that merge into a single peak above T_{MI}.

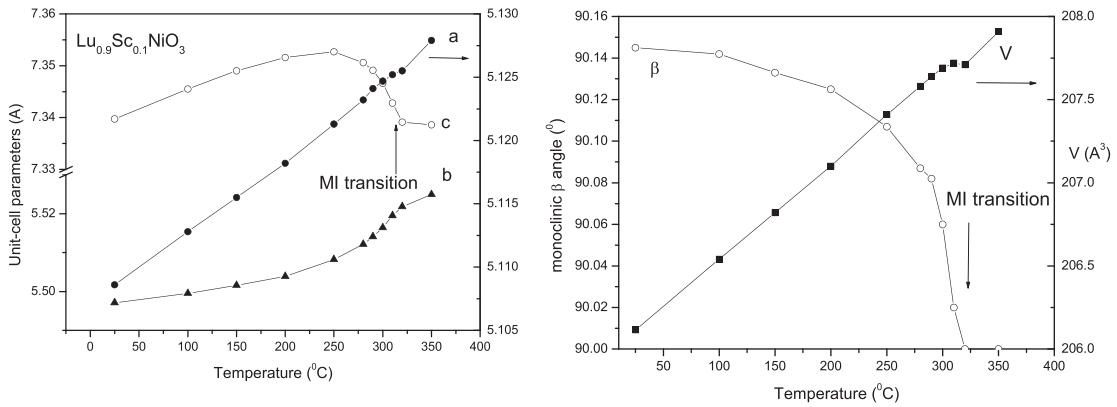

Figure 3. Temperature variation of the unit-cell parameters and volume across the MI transition (T_{MI} = 320 °C). Immediately above T_{MI} the symmetry becomes orthorhombic, and the monoclinic angle abruptly falls to 90°.

Table 1. (a) Structural parameters for $Lu_{0.9}Sc_{0.1}NiO_3$ from SXRD data at 25 °C, sg $P2_1/n$; a = 5.1086(1), b = 5.4971(1), c = 7.3397(2) Å, β = 90.146 (2)°. (b) Structural parameters for $Lu_{0.9}Sc_{0.1}NiO_3$ from SXRD data at 350 °C, s.g. *Pbnm*, a = 5.1279(2), b = 5.5249(2), c = 7.3386(2) Å.

Atom	site	x	y	z	B(Å^2)
Lu,Sc	4*e*	0.9786(3)	0.0777(2)	0.2514(5)	0.75(3)
Ni1	2*d*	0.5	0.0	0.0	0.89(7)
Ni1	2*c*	0.5	0.0	0.5	0.89(7)
O1	4*e*	0.0971(2)	0.4798(2)	0.2584(4)	0.1(2)
O2	4*e*	0.6912(4)	0.2919(4)	0.0609(2)	0.7(3)
O3	4*e*	0.1787(4)	0.1856(5)	0.9805(3)	2.1(6)
(b)					
Lu,Sc	4*c*	0.9785(4)	0.0778(2)	0.25	1.21(6)
Ni1	4*b*	0.5	0.0	0.0	1.11(9)
O1	4*c*	0.0918(3)	0.4886(3)	0.25	0.9(4)
O2	8*d*	0.6883(3)	0.3014(3)	0.0341(2)	2.2(4)

Therefore, the crystal structure at 25 °C and below the transition temperature is defined in the $P2_1/n$ symmetry, as proposed for $RNiO_3$ perovskites [7], with characteristic unit-cell parameters $a \approx \sqrt{2}\,a_0$, $b \approx \sqrt{2}\,a_0$ *and* $c \approx 2a_0$, where a_0 defines the unit-cell of the simple cubic perovskite. In this structure Ni1 and Ni2 are located at 2*d* and 2*c* sites, respectively, and O1, O2 and O3 oxygen atoms at 4*e* Wyckoff sites. Table 1(a) lists the main crystallographic parameters at RT. In the crystal structure there are small $Ni1O_6$ and large $Ni2O_6$ octahedra alternating along the three direction, as displayed in figure 1(c). This arrangement has been interpreted as a charge disproportionation effect [7–11, 25]. It is remarkable the small monoclinic β angle at RT, of 90.15°, indicating a strong pseudo-orthorhombic character. This value compares with those reported in $RNiO_3$ (R = Ho, Y, Er and Lu) perovskites, with β angles ranging from 90.08° for R = Y, Ho to 90.16° for $LuNiO_3$ at RT [9].

Above T_{MI}, in the metallic region, the crystal framework corresponds to the standard *Pbnm* orthorhombic superstructure of perovskite, with a single Ni atom at 4*b* sites and two O1 and O2 atoms at 4*c* and 8*b* Wyckoff positions, respectively (table 1(b)). This is the conventional description of the $GdFeO_3$-type perovskite structure [1].

The variation of the structural parameters across the phase transition at T_{MI} = 320 °C has been investigated from SXRD data (figure 3). The *a* and *b* unit-cell parameters regularly increase in the measured temperature interval; a conspicuous contraction of *c* parameter is realized upon entering the metallic regime across the phase transition. Interestingly, while a decrease of *b* was described for large R perovskites (R = Pr, Nd, Sm) below T_{MI} [27], an increment of the *b* lattice parameter occurs for $RNiO_3$ with smaller rare earths (R = Ho, Y, Er, Lu) [10].

It is interesting to compare the evolution of the interatomic Ni–O bonds between the monoclinic and the orthorhombic phases. Table 2 included the main Ni–O interatomic distances for the two types of NiO_6 octahedra in the $P2_1/n$ structure (at 25 °C), and the single type of NiO_6 octahedron at the *Pbnm* s.g. (at 350 °C). The average ⟨Ni–O⟩ distances indicate that, in the monoclinic model, $Ni1O_6$ octahedron is significantly smaller

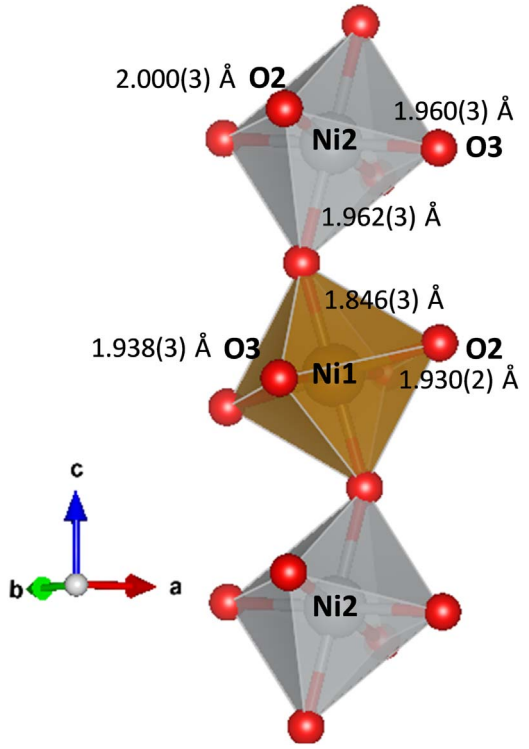

Figure 4. Alternation of expanded and contracted NiO_6 octahedra in the monoclinic, insulating phase below T_{MI}. The three types of oxygen atoms and the corresponding Ni-O distances are displayed.

Table 2. Main bond distances (Å) for monoclinic (at 25 °C) and orthorhombic (at 350 °C) $Lu_{0.9}Sc_{0.1}NiO_3$. For the calculation of the bond valence sums (BVS) the following parameters were used: B = 0.37, $R_0(Lu^{3+})$ = 1.971, $R_0(Sc^{3+})$ = 1.849, $R_0(Ni^{2+})$= 1.654 [35].

T (°C)	25		350
Ni1-O1(x2)	1.846(3)	Ni-O1(x2)	1.895(4)
Ni1-O2(x2)	1.930(2)	Ni-O2(x2)	1.9411(16)
Ni1-O3(x2)	1.938(3)	Ni-O2'(x2)	1.9548(16)
⟨Ni1–O⟩	1.905(1)	⟨Ni–O⟩	1.9304(5)
BVS	3.41(1)		3.16(1)
Ni2-O1(x2)	1.962(3)		
Ni2-O1(x2)	2.000(2)		
Ni2-O1(x2)	1.960(3)		
⟨Ni2–O⟩	1.974(1)		
BVS	2.81(1)		
⟨Ni–O⟩	1.939(2)		

(⟨Ni1–O⟩ = 1.905(1) Å) than $Ni2O_6$ octahedron (⟨Ni2–O⟩ = 1.974(1) Å). This is highlighted in figure 4, illustrating the alternation of both types of contracted and expanded octahedra. The three different Ni–O bond lengths existing at each type of Ni octahedron, in $P2_1/n$, converge to three unique Ni–O distances in the orthorhombic-metallic phase, suggesting that there is a disappearance of the charge disproportionation at the MI transition.

The valences of the cations and anions, BVS = ΣS_{ij}, were estimated using Sij = $\exp[(R_0-R_{ij})/B]$, corresponding to the Brown's Bond-Valence Model [35]. In the monoclinic phase, the BVS for Ni1 and Ni2 are 3.41+ and 2.81+, respectively, significantly above and below the nominal value of 3+, (table 2), indicating the mentioned charge disproportionation, $Ni^{3+\delta}$ and $Ni^{3-\delta}$. In average, the δ value is 0.30, as observed in other members for small rare-earth cations [9].

Figure 5(a) illustrates the thermal variation of the *dc* magnetic susceptibility χ(T) for these three samples. The antiferromagnetic (AFM) transition at T_N is clearly manifested as a kink in χ(T). This singularity broadens up with increasing of the Sc content, probably due to the enhanced lattice distortion with Sc doping. It also

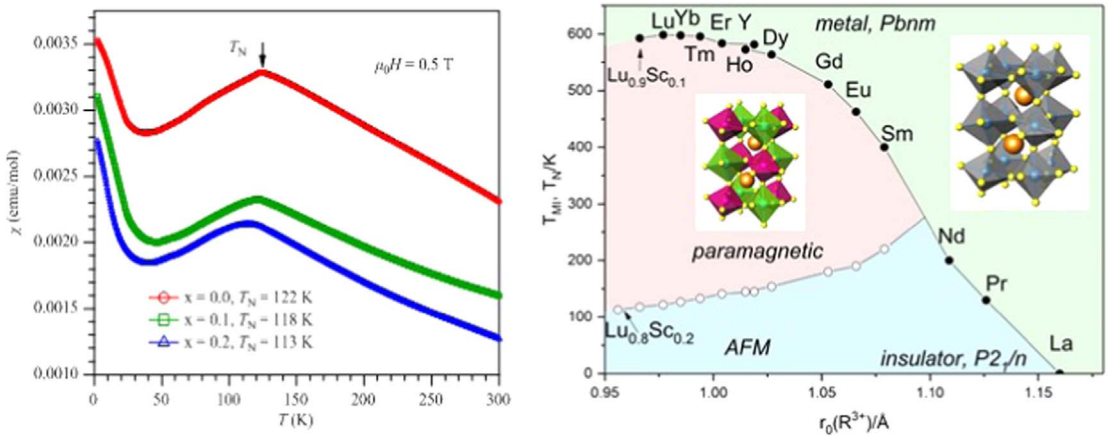

Figure 5. (a) Thermal variation of the dc magnetic susceptibility χ(T) recorded under μ_0H = 0.5 T in field-cooled (FC) mode for $Lu_{1-x}Sc_xNiO_3$ samples. The antiferromagnetic transition temperature (T_N) is marked by the arrow and listed in the figure. (b) Phase diagram for $RNiO_3$ including the two novel members with x = 0.1 and 0.2.

shows that T_N decreases linearly with x in $Lu_{1-x}Sc_xNiO_3$ series; a decrease of the T_N ordering temperature from 122 K (x = 0) to 113 K (x = 0.2) is observed, which is connected with a more distorted perovskite structure with reduced superexchange Ni–O-Ni angles.

Former investigations in the $RNiO_3$ perovskite series described low-spin Ni(III) as ground state [32], also supported in further studies [33]. Moreover, Curie-Weiss fits unveil paramagnetic moments (sufficiently above the onset for magnetic ordering) suggesting a low-spin $3t_{2g}^6 e_g^1$ electronic configuration, S = 1/2, as illustrated for $YNiO_3$ [36]. In complement, the magnetic structures investigated by neutron diffraction at low temperatures disclose ordered magnetic moments compatible with S = ½ [8, 37].

Figure 5(b) shows a complete $RNiO_3$ phase diagram with the novel T_N and T_{MI} points, corresponding to the smallest-sized R^{3+} members of the series. Based on the classical diagram published by Torrance *et al* [5], showing a divergence between the metal-insulator transitions, T_{MI}, and the antiferromagnetic ordering temperature, T_N, for rare-earth sizes slightly smaller than Nd^{3+}, we add a somewhat smaller T_{MI} for $Lu_{0.9}Sc_{0.1}NiO_3$ than that observed for $LuNiO_3$, as well as reduced T_N's for the $Sc_{0.1}$ and $Sc_{0.2}$ members, thus exhibiting the lowest T_N of the full $RNiO_3$ series, given the strongest distortion exhibited by these perovskites.

Conclusions

We have demonstrated that an increased perovskite distortion beyond $LuNiO_3$ is possible in the series $Lu_{1-x}Sc_xNiO_3$. Very high pressure of 10 GPa is required for the stabilization of the novel members. The samples present MI transitions with concomitant structural changes, evolving from a monoclinic phase below T_{MI} to an orthorhombic symmetry in the metallic high-T structure. A dramatic rearrangement of the unit-cell parameters is observed when approaching T_{MI} = 320 °C for x = 0.1. The monoclinic, low-T insulating phase contains two types of Ni octahedra, corresponding to a charge-disproportionation effect. The average charge disproportionation between Ni1 and Ni2 is about ±0.3, as observed in other $RNiO_3$ members with small rare-earth cations. The magnetic properties show an antiferromagnetic ordering with T_N decreasing as the Sc content increases, as corresponds to a more distorted perovskite structure.

Acknowledgments

This work was supported by the Spanish MINECO for funding MAT2017-84496-R. The authors thank ALBA technical staff for making the facilities available for the SXRD experiment 2016091847. JGC is supported by MOST, NSFC and CAS of China (Grants 2018YFA0305700, 11874400, QYZDB-SSW-SLH013) and CAS Interdisciplinary Innovation Team.

ORCID iDs

Jose A Alonso https://orcid.org/0000-0001-5329-1225
Jinguang Cheng https://orcid.org/0000-0002-4969-1960

References

[1] Demazeau G, Marbeuf A, Pouchard M and Hagenmuller P 1971 *J. Solid State Chem.* **3** 582
[2] Ahn C H, Triscone J M and Mannhart J 2003 *Nature* **424** 1015
[3] Torrance J B, Lacorre P, Asavaroengchai C and Metzger R M 1991 *J. Solid State Chem.* **90** 168
[4] Lacorre P, Torrance J B, Pannetier J, Nazzal A I, Wang P W and Huang T C 1991 *J. Solid State Chem.* **91** 225
[5] Torrance J B, Lacorre P, Nazzal A I, Ansaldo E and Niedermayer C 1992 *Phys. Rev.* B **45** 8209
[6] Catalan G 2008 *Phase Transitions* **81** 729
[7] Alonso J A, Martínez-Lope M J, Casais M T, Aranda M A G and Fernández-Díaz M T 1999 *J. Am. Chem. Soc.* **121** 4754
[8] Alonso J A, García-Muñoz J L, Fernández-Díaz M T, Aranda M A G, Martínez-Lope M J and Casais M T 1999 *Phys. Rev. Lett.* **82** 3871
[9] Alonso J A, Martínez-Lope M J, Casais M T, García-Muñoz J L and Fernández-Díaz M T 2000 *Phys. Rev.* B **61** 1756
[10] Alonso J A, Martínez-Lope M J, Casais M T, García-Muñoz J L, Fernández-Díaz M T and Aranda M A G 2001 *Phys. Rev.* B **64** 094102
[11] Fernández-Díaz M T, Alonso J A, Martínez-Lope M J, Casais M T, García-Muñoz J L and Aranda M A G 2000 *Phys. B: Condens. Matter.* **276–278** 218
[12] Medarde M L and 1997 J *Phys. Condens. Matter.* **9** 1679
[13] Giovannetti G, Kumar S, Khomskii D, Picozzi S and van den Brink J 2009 *Phys. Rev. Lett.* **103** 156401
[14] Wu M, Benckiser E, Audehm P, Goering E, Wochner P, Christiani G, Logvenov G, Habermeier H U and Keimer B 2015 *Phys. Rev.* B **91** 195130
[15] Bruno F Y *et al* 2013 *Phys. Rev.* B **88** 195108
[16] Catalano S, Kreisel J, Gibert M, Triscone J M, Íñiguez J and Fowlie J 2017 *Reports Prog. Phys.* **81** 046501
[17] Amow G and Skinner S J 2006 *J. Solid State Electrochem.* **10** 538
[18] Ramadoss K *et al* 2018 *IEEE Electron Device Lett.* **39** 1500
[19] Zhang H T *et al* 2019 *Nat. Commun.* **10** 1651
[20] Wang L, Ju S, You L, Qi Y, Guo Y, Ren P, Zhou Y and Wang J 2016 *Sci Rep.* **5** 18707
[21] Stupakov A, Pacherova O, Kocourek T, Jelinek M, Dejneka A and Tyunina M 2019 *Phys. Rev.* **99** 085111
[22] Li D, Lee K, Wang B Y, Osada M, Crossley S, Lee H R, Cui Y, Hikita Y and Hwang H Y 2019 *Nature* **572** 624–7
[23] Katari V, Babu P D, Mishra S K, Mittal R, Bevara S, Achary S N, Deshpande S K and Tyagi A K 2016 *J. Amer. Ceram. Soc.* **99** 499–506
[24] Sayed F N, Achary S N, Jayakumar O D, Deshpande S K, Krishna P S R, Chatterjee S, Ayyub P and Tyagi A K 2011 *J. Mater. Res.* **26** 567–77
[25] Alonso J A, Martínez-Lope M J, Presniakov I A, Sobolev A V, Rusakov V S, Gapochka A M, Demazeau G and Fernández-Díaz M T 2013 *Phys. Rev.* B **87** 184111
[26] Mercy A, Bieder J, Íñiguez J and Ghosez P 2017 *Nat. Commun.* **8** 1677
[27] Gawryluk D J, Klein Y M, Shang T, Sheptyakov D, Keller L, Casati N, Lacorre P, Fernández-Díaz M T, Rodríguez-Carvajal J and Medarde M 2019 *Phys. Rev.* B **100** 205137
[28] Shamblin J, Heres M, Zhou H, Sangoro J, Lang M, Neuefeind J, Alonso J A and Johnston S 2018 *Nat. Commun.* **9** 86
[29] Bisogni V, Catalano S, Green R J, Gibert M, Scherwitzl R, Huang Y, Strocov V N, Zubko P, Balandeh S and Triscone J M 2016 *Nat. Commun.* **7** 1
[30] García-Muñoz J L, Rodríguez-Carvajal J and Lacorre P 1994 *Phys. Rev.* B **50** 978
[31] García-Muñoz J L, Aranda M A G, Alonso J A and Martínez-Lope M J 2009 *Phys. Rev.* B **79** 1
[32] Fernández-Díaz M T, Alonso J A, Martínez-Lope M J, Casais M T and García-Muñoz J L 2001 *Phys. Rev.* B **64** 1444171
[33] Muñoz A, Alonso J A, Martínez-Lope M J and Fernández-Díaz M T 2009 *J. Solid State Chem.* **182** 1982
[34] Fauth F, Boer R, Gil-Ortiz F, Popescu C, Vallcorba O, Peral I, Fullà D, Benach J and Juanhuix J 2015 *Eur. Phys. J. Plus.* **130** 160
[35] Brown I D and Altermatt D 1985 *Acta Crystallogr.* B **41** 244
[36] Causa M T, Sanchez R D, Tovar M, Alonso J A and Martinez-Lope M J 2003 *Phys. Rev.* B **68** 24429
[37] García-Muñoz J L, Rodríguez-Carvajal J and Lacorre P 1992 *Europhysics Lett.* **20** 241